

RESEARCH ARTICLE

10.1002/2016JA023289

Key Points:

- There are two sources of dayside plasmaspheric hiss. One source is solar pressure, and the other is substorms/small injection events
- Dayside plasmaspheric hiss is typically elliptically polarized and quasi-coherent. Models should include these features in future codes
- The dayside wedge plasmaspheric hiss has a maximum intensity at $L = 2$ to 3, indicating that these waves could be causing the electron slot

Correspondence to:

B. T. Tsurutani,
bruce.tsurutani@jpl.nasa.gov

Citation:

Falkowski, B. J., B. T. Tsurutani, G. S. Lakhina, and J. S. Pickett (2017), Two sources of dayside intense, quasi-coherent plasmaspheric hiss: A new mechanism for the slot region?, *J. Geophys. Res. Space Physics*, 122, 1643–1657, doi:10.1002/2016JA023289.

Received 5 AUG 2016

Accepted 20 DEC 2016

Accepted article online 29 DEC 2016

Published online 10 FEB 2017

Two sources of dayside intense, quasi-coherent plasmaspheric hiss: A new mechanism for the slot region?

Barbara J. Falkowski^{1,2}, Bruce T. Tsurutani¹ , Gurbax S. Lakhina³ , and Jolene S. Pickett⁴ 

¹Jet Propulsion Laboratory, California Institute of Technology, Pasadena, California, USA, ²Department of Physics, Glendale Community College, Glendale, California, USA, ³Indian Institute of Geomagnetism, Navi Mumbai, India, ⁴Physics and Astronomy, University of Iowa, Iowa City, Iowa, USA

Abstract A study of dayside plasmaspheric hiss at frequencies from ~22 Hz to ~1.0 kHz was carried out by using 1 year of Polar data. It is shown that intense, dayside plasmaspheric hiss is correlated with solar wind pressure with $P > 2.5$ nPa. The dayside effect is most prominent in the ~300 to ~650 Hz range. Intense dayside waves are also present during $SYM-H < -5$ nT. The latter is centered at local noon, with the greatest intensities in the $L = 2$ to 3 region. Assuming drift of ~25 keV electrons from midnight to the wave magnetic local time, plasmaspheric hiss is shown to be highly correlated with precursor AE^* and $SYM-H^*$ indices, indicating that the hiss is associated with substorms and small injection events. Our hypothesis is that both sets of waves originate as outer zone ($L = 6$ to 10) chorus and then propagate into the plasmasphere. Fourteen high-intensity dayside plasmaspheric hiss events were analyzed to identify the wave k , polarization, and the degree of coherency. The waves are found to be obliquely propagating, elliptically polarized and quasi-coherent (~0.5 to 0.8 correlation coefficient). It is hypothesized that the dayside plasmaspheric hiss is quasi-coherent because the chorus has been recently generated in the outer magnetosphere and have propagated directly into the plasmasphere. It is possible that the quasi-coherency of the dayside hiss at $L = 2$ to 3 may be an alternate explanation for the generation of the energetic particle slot region.

1. Introduction

Plasmaspheric hiss is generally thought to be a structureless, whistler mode wave with a frequency range between ~20 Hz and ~2.0 kHz, observed by satellites inside the plasmasphere [Dunckel and Helliwell, 1969; Russell et al., 1969; Thorne et al., 1973, 1974; Smith et al., 1974; Solomon et al., 1988; Korth et al., 1986; Gail et al., 1989; Gail and Inan, 1990; Storey et al., 1991; Hayakawa and Sazhin, 1992; Cornilleau-Wehrin et al., 1978, 1993; Santolik et al., 2001; Shinbori et al., 2003; Meredith et al., 2004, 2006; Green et al., 2005; Golden et al., 2012; Tsurutani et al., 2012, 2015; Agapitov et al., 2013, 2014; Summers et al., 2014; Kim et al., 2015; Spasojevic et al., 2015; Li et al., 2015]. It was named for the sound it made when played through a loudspeaker [Thorne et al., 1973]. Several recent papers [Spasojevic et al., 2015; Kim et al., 2015] have stated that plasmaspheric hiss is “incoherent.” This will be addressed in this paper.

Plasmaspheric hiss has been observed during geomagnetic quiet [Carpenter, 1978; Thorne et al., 1977], during substorms [Thorne et al., 1973, 1974, 1977; Meredith et al., 2004; Tsurutani et al., 2011a, 2012, 2015; Agapitov et al., 2014; Kim et al., 2015; Li et al., 2015], and during magnetic storms [Smith et al., 1974; Tsurutani et al., 1975; Bortnik et al., 2009a, 2009b; Kim et al., 2015]. The electromagnetic waves have been observed at all local times, with statistically more intense events on the dayside [Meredith et al., 2004; Tsurutani et al., 2015] than on the nightside. A hiss-like emission has also been detected in high-density plasma regions outside of the plasmasphere, i.e., in plasma “tails” [Chen and Grebowsky, 1974; Chan et al., 1974; Tsurutani et al., 2015].

Thorne et al. [1979] has suggested a local generation of plasmaspheric hiss, with the hiss passing many times through an equatorial amplification region. It has been shown that plasmaspheric hiss is most often present in the dusk sector of the plasmasphere [Tsurutani et al., 2015], indicating that ~10–100 keV electrons drifting into the plasmaspheric bulge may be a source of the waves. Another suggested source of plasmaspheric hiss is electromagnetic whistler mode chorus which is generated near the equatorial plane outside the plasmasphere [Tsurutani and Smith, 1974, 1977; Meredith et al., 2001] with propagation of the chorus into the plasmasphere [Thorne et al., 1973, 1974; Santolik et al., 2001, 2006; Santolik, 2008; Santolik and Chum, 2009; Breneman et al.,

2009; Bortnik *et al.*, 2008, 2009a, 2009b; Tsurutani *et al.*, 2012; Chen *et al.*, 2012; Li *et al.*, 2013]. Specifically, ray tracing studies have been performed that show that it is possible for chorus to propagate into the plasmasphere in the low-altitude region of the plasmapause [Bortnik *et al.*, 2008, 2009a, 2009b; Wang *et al.*, 2011].

Plasmaspheric hiss is a wave that can cyclotron resonate with energetic electrons, leading to their pitch angle scattering and loss to the ionosphere [Kennel and Petschek, 1966]. A “slot region” exists from $L \sim 2$ to ~ 3 where there is a decrease of energetic electron fluxes in the magnetosphere. Lyons *et al.* [1972]; Lyons and Thorne [1973], Albert [1994], Abel and Thorne [1998a, 1998b], and Meredith *et al.* [2006, 2007] have shown that (incoherent) plasmaspheric hiss can cause the formation of the slot.

The purpose of this study is to investigate the plasmaspheric hiss intensification at dayside local times. As noted from above, different studies have indicated different possible sources for plasmaspheric hiss in general. Plasmaspheric hiss has been detected during both quiet and geomagnetic active times. The primary aim of this paper is to attempt to resolve this mystery. Plasmaspheric hiss intensity distributions in L and magnetic local time (MLT) at several frequency ranges, and correlations with AE , $SYM-H$, and solar wind pressure will be studied. Using high-resolution data we will examine the waveforms from a subset of high-intensity events to identify specific properties of the waves, such as their coherence, their angles of propagation relative to the ambient magnetic field, and their ellipticity. All three features are important for modeling wave-particle interactions.

2. Method of Data Analysis

In this study we consider plasmaspheric hiss in the frequency range from ~ 22 Hz to ~ 1 kHz using ~ 1 year (April 1996 to April 1997), of Polar satellite data. The data can be accessed at <http://cdaweb.gsfc.nasa.gov>, NASA's Coordinated Data Analysis Workshop website. The study does not cover the higher-frequency range of $1 \text{ kHz} < f < 2 \text{ kHz}$. This frequency region was specifically not used in order to avoid contamination by lightning-generated sferics.

The plasmasphere was identified by using the electron plasma frequency characteristics in summary wave data plots [Santolik *et al.*, 2001]. The statistical portion of our study covers the region $L = 2$ to $L = 14$ with a focus on the region $L = 2$ to 7 , the location of the plasmasphere. Chorus and magnetosonic waves were removed from the data set by hand inspection [see Tsurutani *et al.*, 2014a]. We performed statistical studies by using the Polar Plasma Wave Instrument data [Gurnett *et al.*, 2004] to determine the occurrence rate as a function of L and magnetic local time (MLT). We calculated the average wave log intensity as a function of L and MLT for the statistical studies.

For the statistical surveys, the ~ 2 kHz bandwidth High Frequency Waveform Receiver (HFWR) data were used. The HFWR covers the frequency range of ~ 22 Hz to ~ 1 kHz in 20 frequency band steps, obtaining ~ 0.45 s snapshots for every ~ 2 min interval [Santolik *et al.*, 2001]. The ~ 2 min interval was then used as the main element for our statistical studies and will hereby be called an “interval.” If plasmaspheric hiss is detected during an interval, it is called a “wave event.” Data were binned by L and MLT with a bin size of $1 L$ by 1 h MLT . The average hiss crossing event was ~ 31 min, with a minimum of ~ 13 min and a maximum of ~ 56 min (information requested by one referee). It should be noted by the reader that these time intervals are due to a combination of the hiss duration and the satellite trajectory through the wave region. Just as chorus events, the emissions themselves can last tens of minutes to hours. Thus, our ~ 2 min samples are not statistically independent. Unfortunately, all satellite plasma wave surveys done in the past suffer from this same limitation. The reader should be aware of this in interpreting the results.

During the course of this study Polar crossed the plasmasphere 2026 times. Of the total 2026 passes, there were ~ 800 passes where the Polar ~ 2 kHz wave data were available. Each pass consists of many ~ 2 min intervals, and thereby many possible wave events. As previously mentioned, these latter ~ 800 passes with many ~ 2 min intervals are the foundation for the statistical part of this study.

For case studies, the high time resolution ~ 0.45 s plasma wave data were analyzed. We use the minimum variance method of Smith and Tsurutani [1976] to determine k , the wave direction of propagation [Verkhoglyadova *et al.*, 2010]. From k and the magnetic field direction B_0 , the wave polarization is determined.

The wave coherence was analyzed for the above cases. A cross correlation of the $B1$ (maximum variance) and $B2$ (intermediate variance) components of the magnetic wave was performed on a selected five wave cycle sample of each event. Individual wave cycles were also analyzed.

The year of study was during solar minimum. During this phase of the solar cycle, there is a paucity of intense interplanetary coronal mass ejection (ICME) magnetic storms [Gonzalez *et al.*, 1994; Tsurutani *et al.*, 2006, 2011b]. Stream-stream interactions forming corotating interaction regions (CIRs) [Smith and Wolfe, 1976] can cause weak magnetic storms [Tsurutani *et al.*, 1995]. However, the high-speed stream proper will be the dominant interplanetary feature causing geomagnetic activity during this part of the solar cycle. The embedded Alfvén waves within the high-speed streams can cause High-Intensity Long-Duration Continuous AE Activity or HILDCAA events [Tsurutani and Gonzalez, 1987; Hajra *et al.*, 2013, 2014] or a series of intense substorms/small injection events with concurrent plasmashet injections.

We will statistically study plasmaspheric hiss using the solar wind pressure from solar wind velocity and density measurements taken from the OMNI website. Since solar wind pressure has an immediate effect on the dayside outer magnetosphere and the energetic $\sim 10\text{--}100$ keV electrons therein, no further time delays were considered. When we consider plasmaspheric hiss associated with substorms, magnetic storms, and plasma injections, we need to determine the AE and SYM-H values assuming midnight injection and gradient drift to the local time of detection. For this part of our study, we use the gradient drift of ~ 25 keV electrons which was shown to be a good measure of chorus delay times by Tsurutani and Smith [1977]. We further note that during the declining phase of the solar cycle and solar minimum, there are often HILDCAA intervals which are the predominant form of geomagnetic activity. These have been shown to be a mixture of continuous substorms and injection events [Tsurutani *et al.*, 1995, 2004]. HILDCAAs are therefore not simply isolated “substorms.” These references are mentioned for the interested reader. We realize that the details of this topic are beyond the scope of the present paper, and thus, no more will be stated here.

It has been shown by Tsurutani *et al.* [2011b] that the solar wind speeds, Alfvénic fluctuation amplitudes, and magnetic field magnitudes are lower in solar minimum than in the declining part of the solar cycle. Thus, one can expect both the CIR storms and the HILDCAAs to be weaker in this study than from intervals from the declining phase of the solar cycle.

We obtained the solar wind data from the OMNI website (<http://omniweb.gsfc.nasa.gov/>). The interplanetary data had already been time adjusted to take into account the solar wind convection time from the spacecraft to the magnetosphere, so no further adjustments were made in this study. We obtained the AE and SYM-H data from the World Data Center (WDC) at Kyoto University (<http://wdc.kugi.kyoto-u.ac.jp/wdc/Sec3.html>). In some cases we use precursor AE and SYM-H values which we will refer to as AE* and SYM-H*.

3. Results

3.1. Solar Wind Pressure Dependence

Polar has an elliptical orbit with perigee at $\sim 2 R_E$ from the center of the Earth and apogee at $\sim 9 R_E$. The orbital period is ~ 17.5 h.

Figure 1a shows the Polar coverage as a function of L (radial direction) and MLT (azimuth) during the interval of study. Approximately 8 h of the Polar orbit is spent in the plasmasphere at distances from $L = 2$ to 7 (indicated by red circles). All magnetic local times (MLTs) were covered.

Figure 1a gives a binning of ~ 2 min intervals. Noon is at the top of the panel and dawn on the right. There is no coverage inside $L = 2$ (shown in white). $L = 2, 4,$ and 7 are indicated for the reader. Each bin has a size $\Delta L = 1$ and $\Delta \text{MLT} = 1$ h. The number of intervals in each bin is indicated by color. The red bins represent a maximum value of 420 intervals, and the lightest yellow color represents a minimum of 35 intervals. Coverage is independent of MLT but varies by L shell. The largest amount of time was spent between $L = 3$ and $L = 4$ as can be noted by the color in Figure 1a.

Figure 1b is the average log intensity of ~ 300 to 1 kHz plasmaspheric hiss found for the coverage given in Figure 1a and is the focus of this paper. The dayside plasmaspheric hiss day-night asymmetry is clearly noticeable in the figure. This dayside intensification is the focus of the present study.

Tsurutani *et al.* [2015] previously noted that some of this dayside plasmaspheric hiss intensification was due to unusually high solar wind pressure intervals. The corresponding plasmaspheric hiss was particularly intense and coherent. To examine the effects of somewhat lower solar wind pressures (allowing more events and better statistics), we have examined intervals when $P > 2.5$ nPa. To show this in a statistical manner for

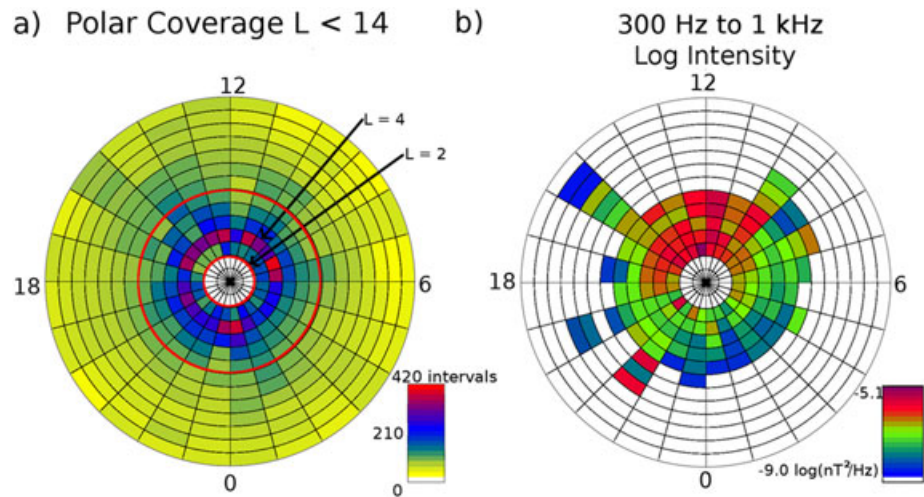


Figure 1. (a) Polar coverage for 1 year of plasmaspheric wave data from ~22 Hz to ~1 kHz as a function of L and MLT. Noon is on the top and dawn is on the right. The coverage extends from L = 2 to L = 14. The legend gives the number of ~2 min intervals for each ΔL - ΔMLT bin. (b) The ~300 Hz to ~1 kHz plasmaspheric hiss average log intensities. Each bin contains log intensities averaged over 1 h MLT and 1 L shell. The color code which gives the intensities is on the bottom right. Reproduced from *Tsurutani et al.* [2015].

various frequency ranges, we have constructed Figure 2. From Figure 2a in a clockwise sense, the frequency ranges are ~22 Hz to ~100 Hz, ~100 Hz to ~300 Hz, ~300 Hz to ~650 Hz, and ~650 Hz to ~1 kHz. For each frequency range, the plasmaspheric hiss average log intensities were calculated for cases when the solar wind pressure P was > 2.5 nPa. The log intensities of the hiss events were averaged over $\Delta MLT = 1$ h and $\Delta L = 1$, the size of each bin. The scale for each panel is on the bottom right. The scale is the same for all panels so that intercomparisons can be made.

Figure 2 visually shows that for $P > 2.5$ nPa, there is clearly a dayside-nightside asymmetry in the average log intensities of the plasmaspheric hiss. The plasmaspheric hiss has higher intensities on the dayside. To get a quantitative estimate of the magnitude of the asymmetries, we have taken the dayside average over all bins (the bin log averages were calculated first) and the nightside average over all bins. We find that the dayside is more intense than the nightside for three of the four frequency ranges. When we calculate how much more intense the dayside was compared to the nightside, we get the following values -3% , $+6\%$, $+12\%$, and $+9\%$ for the ~22–100 Hz, ~100–300 Hz, ~300–650 Hz, and ~650–1000 Hz intervals, respectively. The highest percentage asymmetry is for the ~300–650 Hz frequency range (dayside log average = -6.6 versus nightside log average = -7.5). We will focus on that frequency interval for further studies.

For modeling purposes, the average dayside log intensity is -6.9 , -6.5 , -6.6 , and -7.4 , for the four ascending frequency bands, respectively. The average power is highest in the frequency range ~100 to 650 Hz. However, if one takes the region between 10 and 14 MLT for the 300 to 650 Hz range, a sector where the waves are most intense, we get a log average power of -6.1 .

The plasmaspheric hiss events during $P > 2.5$ nPa were removed from the data set of Figure 1b, and it was noted that the dayside asymmetry was still present. So to try to understand what those remainder events were due to, we studied the plasmaspheric hiss distribution for $P < 2.5$ nPa. Intense events were still present.

3.2. Substorms and Small Injection Events

A number of different interplanetary parameter and geomagnetic indices were studied. One parameter that was found with the dayside plasmaspheric hiss was with $SYM-H < -5$ nT (Figure 3). For high solar wind pressures ($P > 2.5$ nPa) $SYM-H$ has positive values. Thus, the plasmaspheric hiss events using a criteria of $SYM-H < -5$ nT will be almost separate and distinct from those with a selection criteria of $P > 2.5$ nPa. In Figure 3, we show the hiss for ~300 to 650 Hz average log intensities for $SYM-H < -5$ nT.

Figure 3 shows the ~300 Hz to 650 Hz plasmaspheric hiss average log intensities for events with $SYM-H < -5$ nT. The dark green represents the lowest intensities (between -9 and $-8 \log nT^2/Hz$), and the

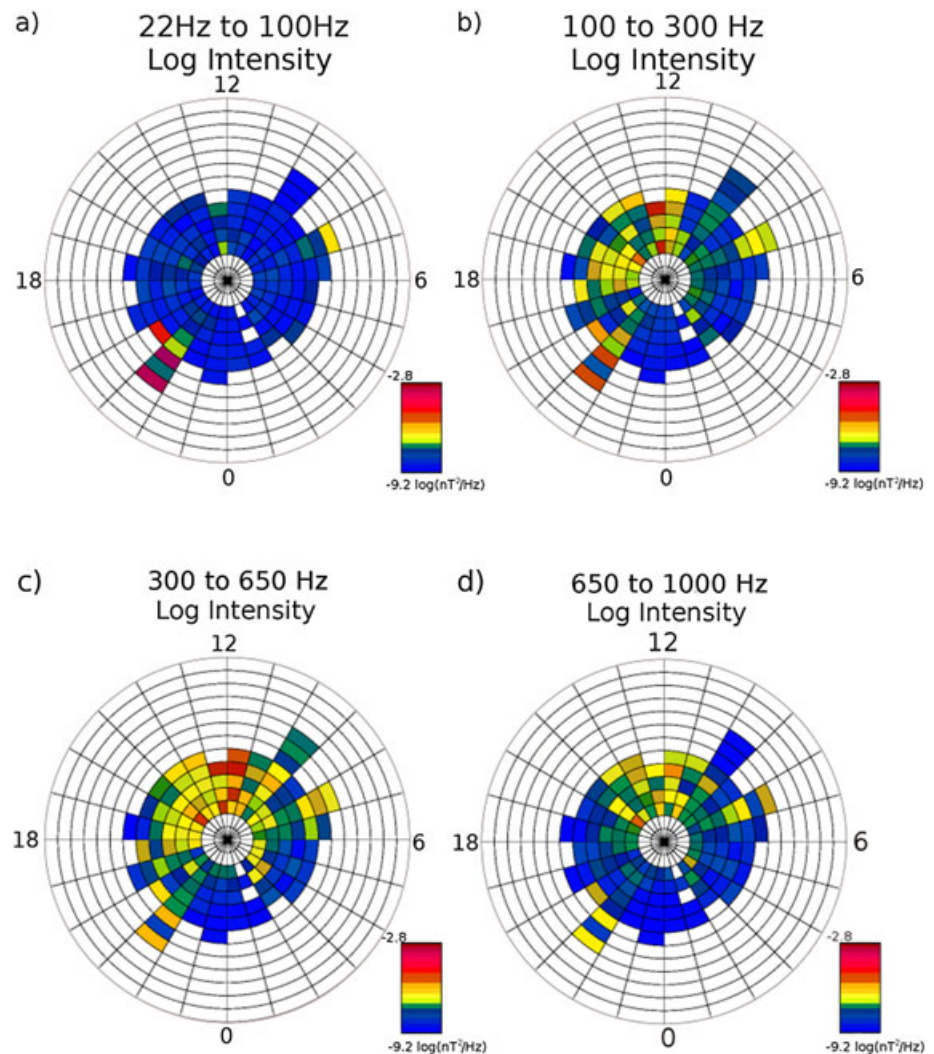


Figure 2. Plasmaspheric hiss during high solar wind pressure conditions ($P > 2.5$ nPa). The pressure measurements were taken from 1 AU satellite measurements. From top left in a clockwise sense is the plasmaspheric hiss in four frequency bands: (a) ~22 to ~100 Hz, (b) ~100 Hz to ~300 Hz, (c) ~300 Hz to ~650 Hz, and (d) ~650 Hz to ~1 kHz.

dark red represents the highest-intensity (between -5 and $-4 \log nT^2/\text{Hz}$) waves. The white indicates a lack of wave events. The vertical scale is magnetic local time with midnight at both the top and the bottom. Noon is in the middle of the figure. The horizontal scale is L with $L = 2$ on the left and $L = 14$ on the right.

There is a dayside region of high-intensity plasmaspheric hiss (the yellow orange and red colors outlined in blue). It has a triangular shape when plotted in MLT versus L. We will call this the “wedge” for shorthand. It ranges from ~0400 to ~1900 MLT at $L \sim 2$ to ~ 3 and then narrows to ~0900 to ~1600 MLT at $L \sim 6$ to ~ 7 . The highest intensities are found from $L = 2$ to 3 in a narrow range from ~1000 to ~1400 MLT or centered at local noon. Intensities in surrounding areas are ~ 1 or ~ 2 orders of magnitude less intense than the high-intensity region. The lowest intensities are detected at high L and from ~0000 MLT to ~0400 MLT and ~1800 MLT to 2400 MLT for $L > 5$. Since none of the plasmaspheric hiss events occurred when $SYM-H < -50$ nT (to be shown in Figure 5), these are not magnetic storm events [Gonzalez et al., 1994]. They will be shown to be related to continuous substorms and small injection events [Tsurutani et al., 2004, 2006].

Figure 4 shows the distribution of AE during the year of study. This is shown by black bars. Intervals of plasmaspheric hiss detection when $SYM-H < -5$ nT within the high-intensity wedge of Figure 3 (grey) are shown by white bars. However, instead of assigning the plasmaspheric hiss the AE value at the time of detection, the local time of the plasmaspheric hiss was used to find the AE value when ~25 keV electrons would have been

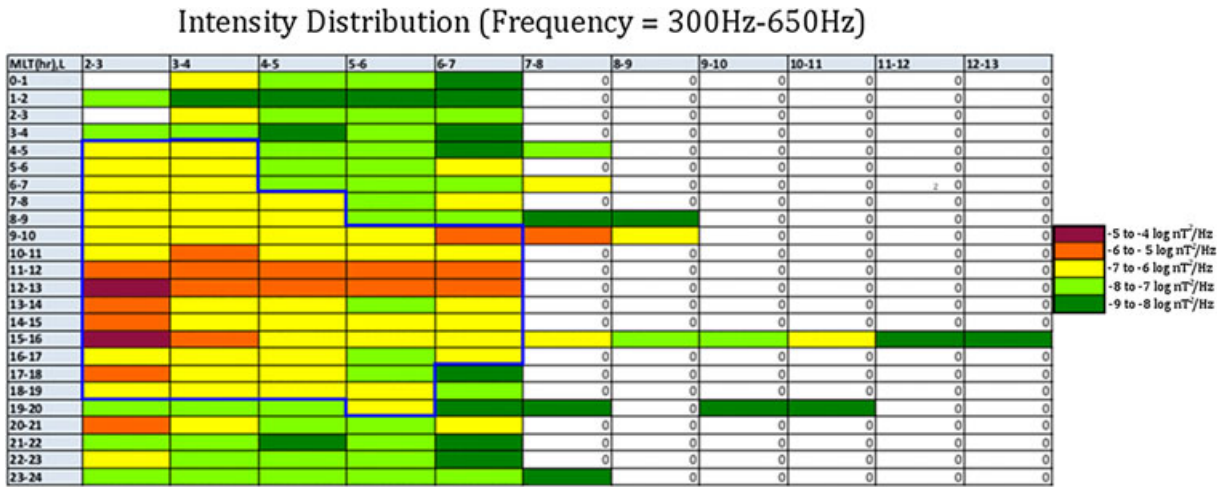


Figure 3. Plasmaspheric hiss average log intensity distribution as a function of MLT and L shell for events during $SYM-H < -5$ nT. MLT is given on the vertical axis, and L is the horizontal axis. Bins are 1 h by 1 L shell. Intensity is represented by color with each color representing 1 order of magnitude. The legend is on the right. The highest intensities (10^{-5} to 10^{-4} $\log nT^2/Hz$) are dark red; the lowest are dark green (10^{-9} to 10^{-8} $\log nT^2/Hz$).

injected into local midnight; e.g., we backdated the hiss AE (AE^*). This particular energy of electrons was chosen because *Tsurutani and Smith* [1977] previously showed that it worked well for identifying chorus delay times from substorm (AE) onsets. For a local time of noon plasmaspheric hiss detection, the electron drift time was ~ 2 h. The hiss percentage occurrence is plotted with the scale on the right.

This plasmaspheric hiss AE^* distribution is clearly different than the background AE distribution. Dayside plasmaspheric hiss in the wedge of Figure 3 occurs within high AE^* intervals, assuming delay times for ~ 25 keV electrons drifting from midnight to the local time of plasmaspheric hiss detection.

Figure 5 shows the distribution of $SYM-H^*$ values during the plasmaspheric hiss events for the wedge of Figure 3. A ~ 25 keV electron delay time was assumed for the electrons drifting from midnight to the local time of plasmaspheric hiss detection. This is the same delay time method that was used previously in Figure 4.

The plasmaspheric hiss occurs only when the preceding $SYM-H^*$ is negative, ranging from ~ -45 nT to ~ 0 nT. Since magnetic storms are events where $SYM-H < -50$ nT [Gonzalez et al., 1994], none of these events are storm events. This result is in agreement with that of Figure 4, that the dayside plasmaspheric hiss is related to substorms and small injection events (HILDCAAs). As previously mentioned the data for our study were

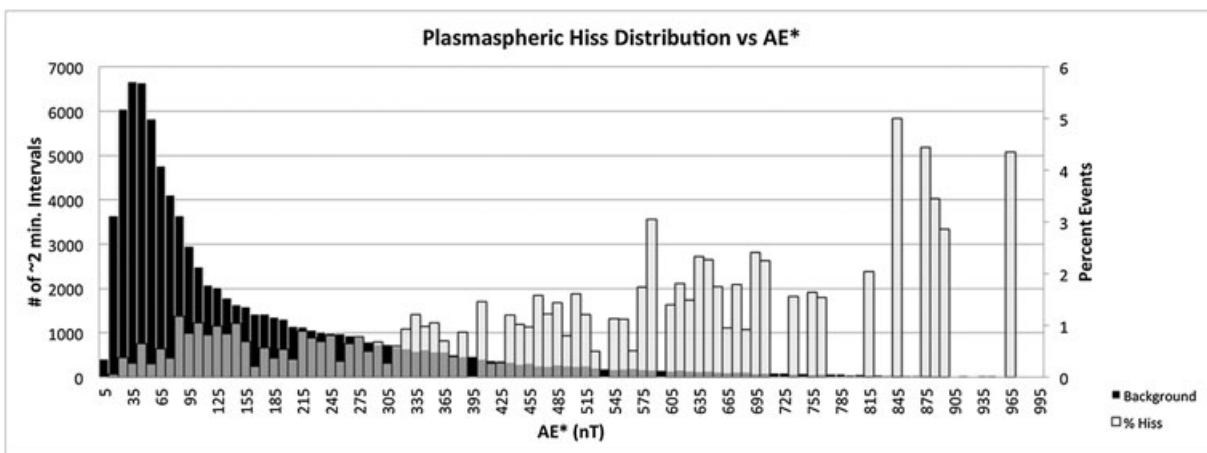


Figure 4. The distribution of AE values for the 1 year interval of study (black bins). The vertical scale is number of ~ 2 min intervals for each AE value bin. Displayed in grey are hiss events with $SYM-H < -5$ nT in the wedge of Figure 3. An AE precursor (AE^*) time was applied to account for ~ 25 keV electron drift to the local time of the plasmaspheric hiss detection.

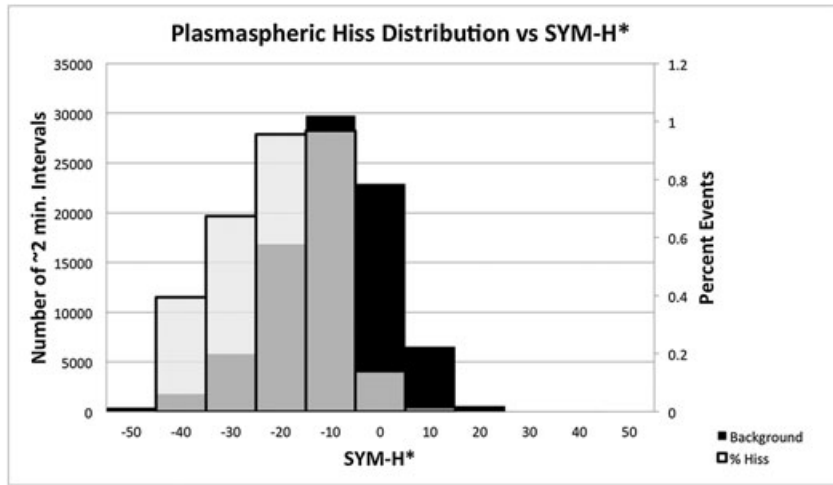


Figure 5. Distribution of SYM-H* during plasmaspheric hiss events. The black histogram is the distribution of SYM-H values over the entire year. The grey histogram is the percentage of SYM-H* values found in the wedge region in Figure 3 delayed in time associated with a gradient drift of ~25 keV electrons in the outer magnetosphere to the MLT of the hiss event.

taken during solar minimum where there is a general lack of ICME magnetic storms. The prime causes of geomagnetic activity during this phase of the solar cycle are high-speed solar wind streams and related High-Intensity Long-Duration Continuous AE Activity (HILDCAA) intervals [Tsurutani et al., 1995, 2006; Hajra et al., 2013]. We caution the reader that the results may be different than those taken during the maximum phase of the solar cycle.

3.3. Waveform Analysis

Detailed information of plasmaspheric hiss properties for the dayside waves were also studied, the results of which should be taken into account for future construction of wave-particle interaction models. Thus, 14

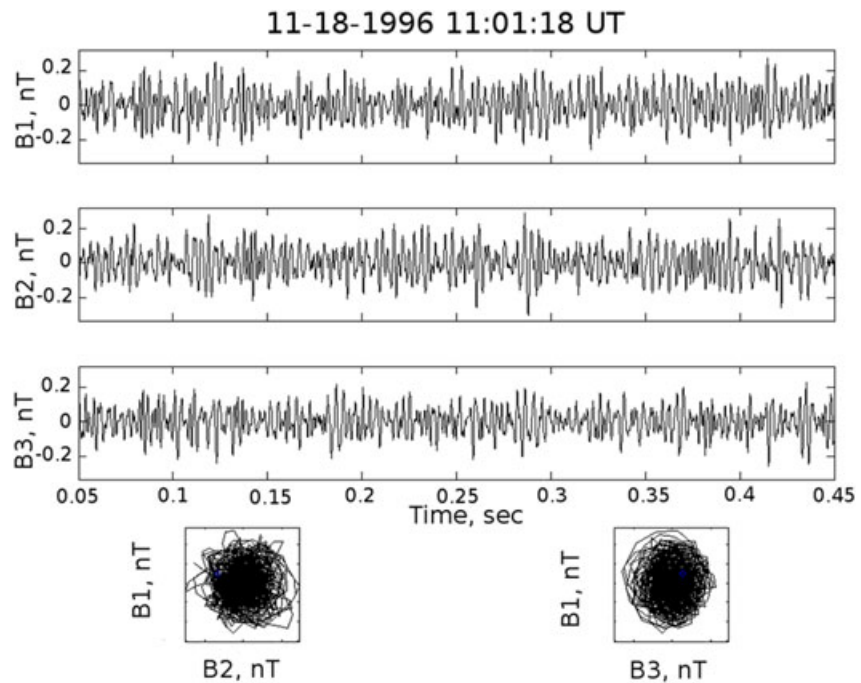


Figure 6. A typical high-intensity dayside wave interval. The plasmaspheric hiss was detected on 18 November 1996 at 1101 UT. The Polar satellite was at 1020 MLT and at L = 3.0. The top three panels show the B1, B2, and B3 magnetic field components, respectively. The B1-B2 hodogram is in the bottom left. The B1-B3 hodogram is in the bottom right.

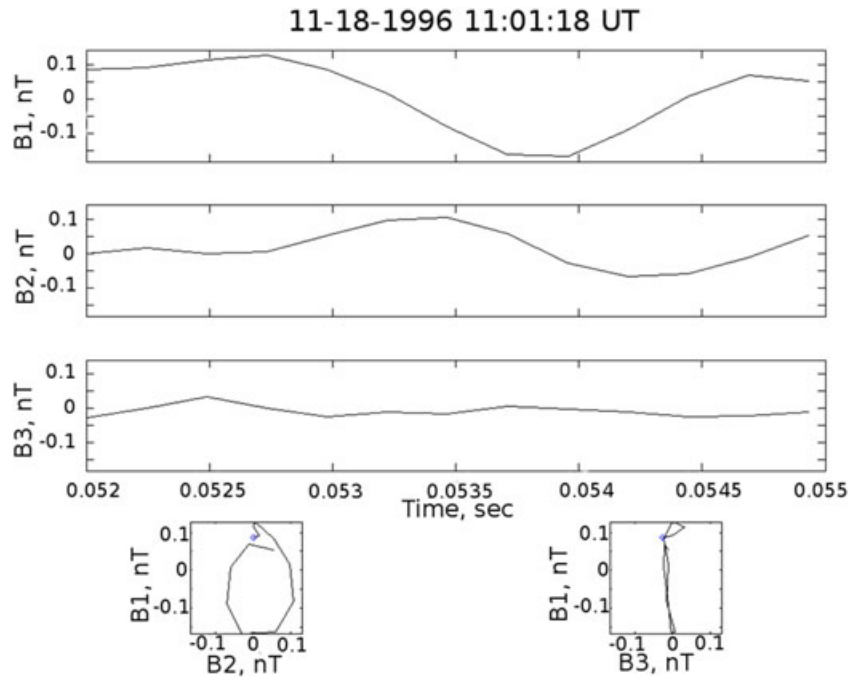


Figure 7. A single wave cycle of the plasmaspheric hiss shown in Figure 6. The format is the same as in Figure 6.

~0.45 s snapshots of the highest-intensity events with $SYM-H < -5$ nT (the wedge region) were selected for more detailed study. The highest-intensity emissions were selected. From the 14 intervals, events with greater than ~100 cycles were first analyzed by using the minimum variance technique. Cross correlations were calculated between the B1 and B2 magnetic field components to determine the degree of coherence.

Figure 6 shows ~0.4 s of a typical high-intensity wave interval in minimum variance coordinates. The event was observed on 18 November 1996. At the time Polar was at $L \sim 3$, 1007 MLT, and the $SYM-H$ at the time was -22 nT. The first three panels show the three magnetic field components as a function of time. The B1 component shown in Figure 6 (top) has a maximum wave amplitude of ~2.5 nT. The other two components are comparable but slightly smaller in magnitude.

Figure 6 (bottom left) shows a graph of B1 versus B2, the maximum variance direction field component plotted against the intermediate variance direction field component, respectively. Over many cycles the polarization appears to be nearly circular. However, this panel shows many superposed wave cycles, and this supposition is not conclusive. Smaller time intervals need to be studied to better determine the wave polarization.

Figure 6 (bottom right) is B1 plotted against B3, the maximum variance component plotted against the minimum variance component. If the waves are planar in nature, this type of distribution could indicate a somewhat isotropic distribution of wave propagation directions.

Figure 7 shows the results of a minimum variance analysis of a single cycle of the plasmaspheric hiss shown in Figure 6. The format is the same. Figure 7 (top) is the B1 wave component with amplitude of about 0.15 nT. The B2 component has a value of ~0.10 nT. The plot in Figure 7 (bottom left) is the B1-B2 hodogram showing that the wave is elliptically polarized. The direction of wave propagation is 11.9° from B_0 . The ambient magnetic field is into the paper; thus, the wave is right-hand polarized.

Figure 7 (bottom right) indicates that the wave cycle is planar in nature. This supports the hypothesis that the hodogram of Figure 6b was composed of many planar waves propagating at a variety of angles relative to the spacecraft.

The wave cycle in Figure 7 is typical of the ~100 cycles of waves that were analyzed. Almost all were elliptically polarized. The average value of λ_1 / λ_2 was 3.9. However, many angles of propagation were noted, ranging from 10° (quasiparallel propagation) to $\sim 60^\circ$ (highly oblique propagation or a mixture of several

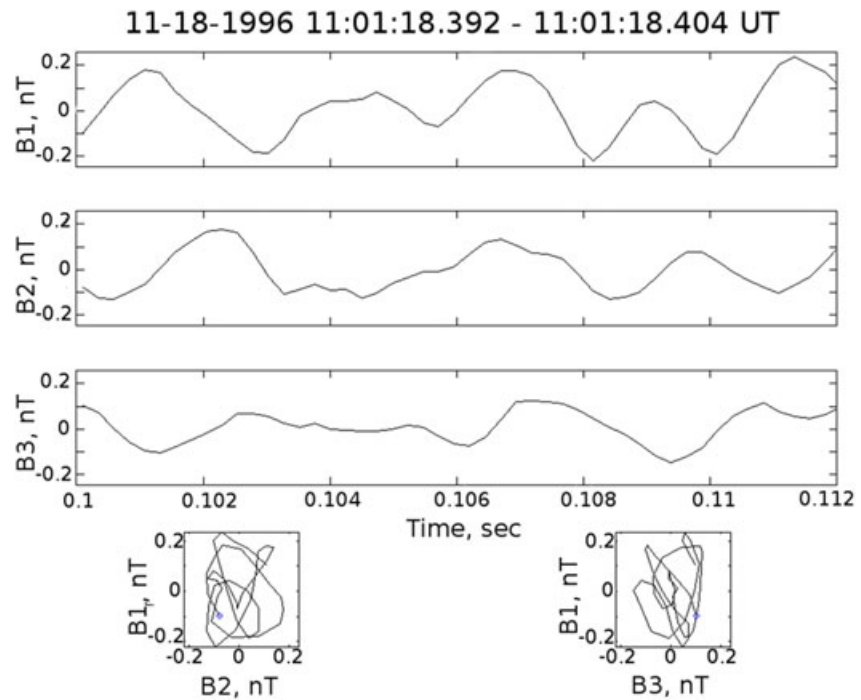


Figure 8. Five consecutive wave cycles from the event in Figure 6. The format is the same as in Figure 6.

waves present at the same time) relative to B_0 . Essentially, no clear direction of propagation was found. This too is in support of a distribution of multidirectional wave propagation indicated in Figure 6.

Figure 8 shows a series of five consecutive cycles. This interval is also taken from Figure 6. From the top two panels it is easy to see that there is a definite relationship between B1 and B2, but neither forms are sinusoidal in nature. Figure 8 (bottom left) shows that the individual cycles are elliptically polarized. Similar behavior has been observed in plasmaspheric hiss at high positive *SYM-H* (reported in *Tsurutani et al.* [2015]) but not at negative *SYM-H*.

When the minimum variance analysis is performed on individual cycles it is found that they propagate at the following angles with respect to B_0 : 21°, 37°, 63°, 26°, and 57°. The waves appear to be propagating to the spacecraft from many angles.

The approximate frequency of the waves is ~420 Hz, which is in the range of values included in the statistical analysis in Figure 2. Other high-intensity events analyzed in high time resolution also showed elliptical polarization.

The panels of Figure 9, from top to bottom, are the B_0 field magnitude, B1 and B2 superposed on top of each other, and the cross correlation between B1 and B2 as a function of lag.

Figure 9 (middle) with B1 superposed on top of B2 indicates that there are distinct correlations between the two field components, but they are not one to one. One possible explanation is that there are several wave sources present and the search coil sensors are detecting this wave superposition.

Figure 9 (top) indicates that there are small B_0 variations. These are due to the magnetic field aligned components of the obliquely propagating waves superposed on the ambient magnetic field.

Figure 9 (bottom) shows the cross-correlation coefficient between the B1 and B2 component of the waves. The correlation at 0.25 and 1.25 wavelength lag are ~0.8. The correlation coefficient is generally lower at larger lags. The wave is thus quasi-coherent. In this example Polar was at $L \sim 3$. There are numerous examples of quasi-coherent plasmaspheric hiss at low L in this in situ data. Quasi-coherent waves are characterized by “intermittent” coherence lasting several cycles as described by *Tsurutani et al.* [2009, 2011a, 2011b]. By intermittent coherence, we mean that the waves are quasi-coherent for a few cycles, then low in coherence, then quasi-coherent again for a few cycles. No particular time intervals between quasi-coherent intervals were noted.

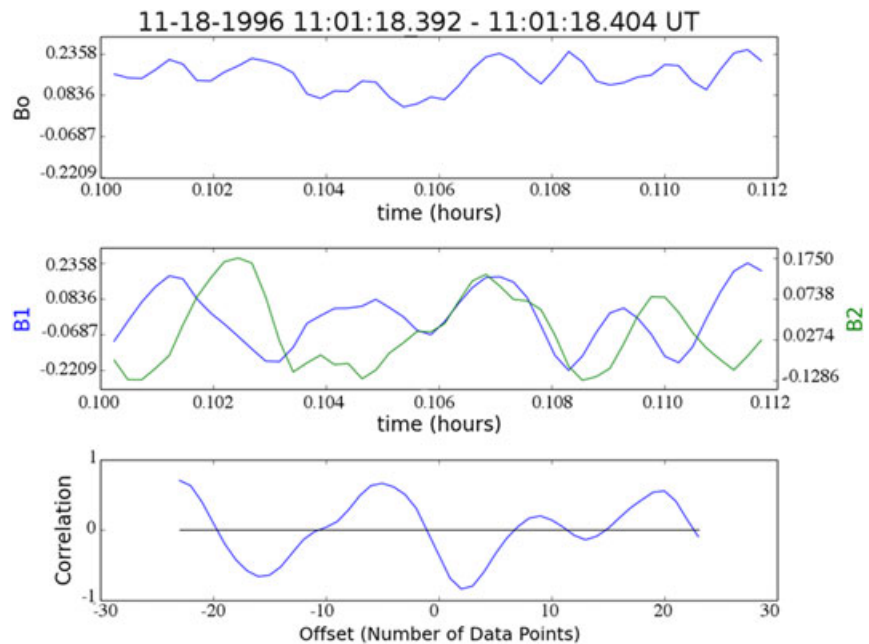


Figure 9. (top) The magnetic field magnitude, B_0 . (middle) The B1 and B2 components superposed on top of each other. (bottom) The cross correlation of B1 and B2 as a function of lag.

All 17 high-intensity wave intervals were examined in detail, and the above results are typical of our findings. The waves are propagating obliquely to the ambient magnetic field, are $\sim 2:1$ elliptically polarized, and are quasi-coherent with a correlation between B1 and B2 of 0.5 to 0.8. These properties should be incorporated in any realistic wave-particle interaction model.

4. Summary

The following are the main findings of our study of dayside plasmaspheric hiss:

1. Statistical analyses of 1 year of Polar plasmaspheric hiss events (April 1996 to April 1997) indicate that in the frequency range of ~ 300 Hz to ~ 650 Hz, plasmaspheric hiss is ~ 1 order of magnitude more intense on the dayside than on the nightside (Figure 1). The ~ 100 Hz to ~ 350 Hz and ~ 650 Hz to 1000 Hz frequency ranges showed similar but smaller-intensity asymmetries. There was little or no asymmetry detected in the ~ 22 Hz to ~ 100 Hz frequency range.
2. Dayside plasmaspheric hiss intensifications are detected during high solar wind pressure conditions ($P > 2.5$ nPa), accounting for part of the dayside asymmetry (Figure 2).
3. During $SYM-H < -5$ nT, the region of enhanced dayside plasmaspheric hiss ranges from ~ 0500 to ~ 1900 MLT at L ~ 2 to ~ 3 and then narrows to ~ 0900 to ~ 1600 MLT at L ~ 6 to ~ 7 (Figure 3). The peak enhancement is at approximately local noon. We have called this triangular shaped region the wedge for shorthand. It is noted that the most intense plasmaspheric hiss is detected at the location of the energetic electron slot region.
4. The wedge in item 3 is correlated with prior enhanced AE (AE^*) and $SYM-H$ ($SYM-H^*$), indicating a substorm or small midnight injection origin of ~ 25 keV electrons to generate outer zone chorus [Tsurutani and Smith, 1977]. In our scenario we presume this chorus to be the origin of the hiss. A time delay was assumed for the electrons to drift to the dayside local time where the hiss was detected (Figures 4 and 5).
5. Intense wedge plasmaspheric hiss is elliptically polarized (Figure 7), obliquely propagating (Figure 8), and quasi-coherent with B1-B2 correlation coefficients of 0.5 to 0.8 (Figure 9). Specific cases studied indicate a wide distribution of propagation angles (Figure 6). Parallel propagating plasmaspheric hiss was found to be circularly polarized (not shown). Plasmaspheric hiss was found to typically be elliptically polarized by a ratio of 2 to 1. For a theoretical discussion of elliptically polarized whistler mode waves we refer the reader to Remya et al. [2016].

5. Discussion and Conclusions

There have been recent previous results on plasmaspheric hiss day/night intensity asymmetry [Meredith *et al.*, 2007; Tsurutani *et al.*, 2015], the wave's propagation angles [Agapitov *et al.*, 2013; Tsurutani *et al.*, 2015], and its geomagnetic activity dependence [Meredith *et al.*, 2007; Golden *et al.*, 2012; Spasojevic *et al.*, 2015; Kim *et al.*, 2015; Li *et al.*, 2015]. Golden *et al.* [2012] and Tsurutani *et al.* [2015] addressed solar wind pressure dependence as well. All of the above results give a very nice picture of plasmaspheric hiss properties that will help enable wave-particle interaction modeling. What is new in this paper that can be used to aid in improving such modeling?

By looking at specific high solar wind pressure intervals ($P > 2.5$ nPa) alone, we have been able to find dayside plasmaspheric hiss intensifications. Also by assuming ~ 25 keV electron drifts from approximately midnight to the plasmaspheric hiss local time, the AE^* and $SYM-H^*$ features clearly indicate substorm or small injection event (nonstorm events) dependence, consistent with midnight injection of energetic electrons. Thus, for the first time we have shown that dayside plasmaspheric hiss has two distinct and separable origins.

Some caveats should also be added to the above statements. Plasmaspheric hiss can also be generated in the duskside plasmaspheric bulge and in plasma plumes [Tsurutani *et al.*, 2015] as well as possibly being generated by a recirculation through the equatorial region [Thorne *et al.*, 1979]. It should also be noted that a relationship with AE does not necessarily imply only substorm dependence. Tsurutani *et al.* [2004] have shown that during HILDCAAs (during the declining phase of the solar cycle) injection events also occur in addition to the classic Akasofu [1964] optical substorms. At this time this is still not well understood. Thus, we have added the phrase "small injection events" in the text (small in contrast to magnetic storms which are large injection events [Gonzalez *et al.*, 1994]).

Using intense dayside plasmaspheric hiss events, it is found that the waves are typically elliptically polarized. A wide range of propagation directions are found, indicating either a multisource nature of the waves in the inner plasmasphere or a single unducted source with wave reflections. Elliptical polarization, and not the standardly assumed circular polarization (used in most models), will affect wave-particle interactions (causing a lessening of the efficiency).

Some of the recent past authors have used the phrases "unstructured" [Spasojevic *et al.*, 2015] and "incoherent" [Kim *et al.*, 2015] to describe plasmaspheric hiss. However, we have shown that under certain conditions plasmaspheric hiss can be quasi-coherent. This can make an important and large difference in wave-particle interaction calculations. In fact, wave coherency may be equal in importance as wave intensity. It has been shown that for the case of outer zone chorus, wave coherency can increase the pitch angle diffusion rate of energetic electrons by 3 orders of magnitude [Tsurutani *et al.*, 2009, 2011b; Lakhina *et al.*, 2010; Bellan, 2013] compared to the incoherent wave-particle scattering rate [Kennel and Petschek, 1966; Tsurutani and Lakhina, 1997]. Thus, low-amplitude coherent waves can have an equal particle pitch angle scattering effect as high-amplitude incoherent waves. Coherent chorus waves have been used to explain the extremely rapid pitch angle diffusion needed for ~ 10 to 100 keV electron microburst precipitation [Tsurutani *et al.*, 2013].

5.1. Sources of the Dayside Plasmaspheric Hiss Under High Solar Wind Pressure and Associated With Geomagnetic Activity

It is thought that the most likely source for both types of dayside plasmaspheric hiss is dayside outer zone magnetospheric chorus. Chorus has been shown to be generated by solar wind compression of the outer magnetosphere and remnant ~ 10 –100 keV particles therein [Kokubun, 1983; Gail and Inan, 1990; Shinbori *et al.*, 2003; Tsurutani *et al.*, 2008, 2014b, 2016; Remya *et al.*, 2015]. Chorus is also well known to be substorm dependent [Tsurutani and Smith, 1974, 1977; Meredith *et al.*, 2001, 2004]. Chorus propagation into the plasmasphere has been shown by a number of ray tracing works [Bortnik *et al.*, 2008, 2009a, 2009b; Parrot *et al.*, 2003; Delport *et al.*, 2012].

The quasi-coherency of the waves found in the dayside plasmaspheric hiss wedge supports the idea that the waves were recently generated and have propagated into the plasmasphere. A previous study of plasmaspheric hiss detected in plasma plumes indicated the same (actually higher) level of the wave coherency [Tsurutani *et al.*, 2015]. The argument was made that this plasmaspheric hiss was generated by ~ 10 –100 keV electrons drifting through the high-density plasma plumes and was thus freshly generated waves.

What about the local time dependence of plasmaspheric hiss associated with solar wind pressure? *Spasojevic et al.* [2015] noted a distribution centered at local noon, similar to the one found here. *Kim et al.* [2015] found two different locations: a prenoon sector peak associated with IMF B_z (substorms and small injection events?) and a postnoon sector peak associated with V_{sw} (solar wind pressure?). At this time we do not have a very good explanation for the slight differences between the results of the different studies. They were done at different times, and as previously mentioned, none of the studies are strictly statistically significant. We do offer one possible explanation of the local noon peak found in the present study however. During the minimum phase of the solar cycle, continuous injection of ~ 10 to 100 keV electrons at midnight occurs through HILDCAAs. Drift shell splitting of ~ 10 to 100 keV electrons [*Roederer and Zhang*, 2014] as the electrons drift to the outer dayside magnetosphere into minimum B pockets will leave the energetic electrons with high $T_{\perp}/T_{\parallel} > 1$ anisotropies there. A search for such electron anisotropies and chorus in minimum B pockets during HILDCAA intervals would be a test for this idea.

There is good agreement that the intensity peak of hiss is located quite deeply inside the plasmasphere. *Spasojevic et al.* [2015] found a plasmaspheric hiss intensity peak between $L = 3.25$ and 3.5 ; *Kim et al.* [2015] found it between $L = 3$ to 5 . Here in this paper we find a maximum located between $L = 2$ and 3 . If chorus is indeed the origin of plasmaspheric hiss, ray tracing can be employed to determine where in the outer magnetosphere any particular hiss wave event had its origin [see *Bortnik et al.*, 2008]. This would be an additional test of the idea of chorus origination.

The very nice work of *Li et al.* [2015] following the seminal works of *Meredith et al.* [2006, 2007] have indicated that the dominant power of plasmaspheric hiss occurs in the frequency range below ~ 550 Hz. Our present results are in agreement with this finding. Our peak dayside plasmaspheric hiss intensity occurs in the ~ 100 Hz to ~ 300 Hz and ~ 300 Hz to ~ 650 Hz frequency ranges.

5.2. A New Scenario for the Electron Slot

We have illustrated the difference in coherency and wave propagation results that one gets using different time intervals of the waves. It is on the smallest scale that energetic particles resonate with the waves, not the aggregate or average wave properties. Thus, when one considers modeling wave-particle interactions, one should look at the partial cycle wave intervals to understand particle reactions.

Meredith et al. [2006, 2007] have analyzed plasmaspheric hiss as a possible wave emission responsible for electron loss from the radiation belts, particularly the slot region ($2 < L < 3$). In their modeling they had assumed incoherent waves and assumed that the interaction occurred at all local times over long time periods. Here we find that substorm and small injection events cause intense quasi-coherent plasmaspheric hiss in the dayside sector. The maximum plasmaspheric hiss intensity occurs at $L = 2$ to 3 , the electron slot region. The main difference between this present hypothesis and that of the "steady drizzle" model is in this case electron precipitation will occur when there are substorms/injection events (HILDCAAs) populating the outer radiation belts with ~ 10 to 100 keV electrons. So in this picture, the losses will be sporadic. We urge modelers to consider examining this alternate hypothesis. The question is not which process is the "correct one." Certainly both processes are occurring. The question is which process is more dominant and under what conditions.

We note that there is a new result by *Verkhoglyadova et al.* [2016] who have found evidence for subauroral enhanced ionization in the E layer. The authors were studying a (pure) high-speed solar wind stream ionospheric response, much like we expect is dominating the interplanetary causes of our plasmaspheric hiss statistical data here. *Verkhoglyadova et al.* [2016] have surmised that the precipitation is due to $E > 10$ keV electrons.

One might ask why plasmaspheric hiss is intensified on the dayside and not the nightside during substorm/small injection events? It has been shown that on the nightside chorus propagating away from its equatorial generation region gets quickly damped [*Tsurutani and Smith*, 1974, 1977; *Meredith et al.*, 2004]; thus, the waves will not reach the low altitudes necessary to enter the plasmasphere.

We offer one final caveat. Most of the plasmaspheric hiss surveys have been performed with data taken during the solar declining phase/solar minimum intervals. During solar maximum when geomagnetic activity is associated with ICME storms [*Tsurutani and Gonzalez*, 1997], the nightside plasma injections will be far deeper into the magnetosphere. Thus, the sources and location of plasmaspheric hiss may be different during this epoch of the solar cycle.

Acknowledgments

Portions of this research were performed at the Jet Propulsion Laboratory, California Institute of Technology, under contract with NASA. The Polar plasma wave data can be accessed at <http://cdaweb.gsfc.nasa.gov>. The solar wind data were obtained from the OMNI website at <http://omniweb.gsfc.nasa.gov/>. The AE and SYM-H data used in this study were obtained from the WDC for Geomagnetism at Kyoto University (<http://wdc.kugi.kyoto-u.ac.jp/wdc/Sec3.html>). G.S.L. thanks the National Academy of Sciences, India, for support under the NASI-Senior Scientist Platinum Jubilee Fellowship Scheme.

References

- Abel, B., and R. M. Thorne (1998a), Electron scattering loss in Earth's inner magnetosphere: 1. Dominant physical processes, *J. Geophys. Res.*, *103*, 2385–2396, doi:10.1029/97JA02919.
- Abel, B., and R. M. Thorne (1998b), Electron scattering loss in Earth's inner magnetosphere: 2. Sensitivity to model parameters, *J. Geophys. Res.*, *101*, 2397–2407, doi:10.1029/97JA02920.
- Agapitov, O., A. Artemyev, V. Krasnoselskikh, Y. V. Khotyaintsev, D. Mourenas, H. Breuillard, M. Balikhin, and G. R. Rollard (2013), Statistics of whistler mode waves in the outer radiation belt: Cluster STAFF-SA measurements, *J. Geophys. Res. Space Physics*, *118*, 3407–3420, doi:10.1002/jgra.50312.
- Agapitov, O. V., A. V. Artemyev, D. Mourenas, Y. Kasahara, and V. Krasnoselskikh (2014), Inner belt and slot region electron lifetimes and energization rates based on Akebono statistics of whistler waves, *J. Geophys. Res. Space Physics*, *119*, 2876–2893, doi:10.1002/502014JA019886.
- Akasofu, S.-I. (1964), The development of the auroral substorm, *Planet. Space Sci.*, *12*, 273–282, doi:10.1016/0032-0633(64)90151-5.
- Albert, J. M. (1994), Quasi-linear pitch angle diffusion coefficients: Retaining high harmonics, *J. Geophys. Res.*, *99*, 23,741–23,745, doi:10.1029/94JA02345.
- Bellan, P. M. (2013), Pitch angle scattering of an energetic magnetized plasma by a circularly polarized electromagnetic wave, *Phys. Plasmas*, *20*, 042117.
- Bortnik, J., R. M. Thorne, and N. P. Meredith (2008), The unexpected origin of plasmaspheric hiss from discrete chorus emissions, *Nature*, *452*, doi:10.1038/nature06741.
- Bortnik, J., W. Li, R. M. Thorne, V. Angelopoulos, C. Cully, J. Bonnell, O. LeContel, and A. Roux (2009a), An observation linking the origin of plasmaspheric hiss to discrete chorus emissions, *Science*, *324*, 775–778, doi:10.1126/science.1171273.
- Bortnik, J., R. M. Thorne, and N. P. Meredith (2009b), Plasmaspheric hiss overview and relation to chorus, *J. Atmos. Sol. Terr. Phys.*, *71*, 1636–1646, doi:10.1016/j.jastp.2009.03.023.
- Breneman, A. W., C. A. Kletzing, J. Pickett, J. Chum, and O. Santolik (2009) Statistics of multispacecraft observations of chorus dispersion and source location, *J. Geophys. Res.*, *114*, A06202, doi:10.1029/2008JA013549.
- Carpenter, D. L. (1978), New whistler evidence of a dynamo origin of electric fields in the quiet plasma, *J. Geophys. Res.*, *83*, 1558–1564, doi:10.1029/JA083iA04p01558.
- Chan, K.-W., R. E. Holzer, and E. J. Smith (1974), A relation between ELF hiss amplitude and plasma density in the outer plasmasphere, *J. Geophys. Res.*, *79*(13), 1989–1993, doi:10.1029/JA079i013p01989.
- Chen, L., J. Bortnik, W. Li, R. M. Thorne, and R. B. Horne (2012), Modeling the properties of plasmaspheric hiss: 1. Dependence on chorus wave emission, *J. Geophys. Res.*, *117*, A05201, doi:10.1029/2011JA017201.
- Chen, A. J., and J. M. Grebowsky (1974), Plasma tail interpretations of pronounced detached plasma regions measured by OGO 5, *J. Geophys. Res.*, *79*, 3851–3855, doi:10.1029/JA079i025p03851.
- Cornilleau-Wehrin, N., R. Gendrin, F. Lefeuvre, M. Parrot, R. Gard, D. Jones, A. Bahnsen, E. Ungstrup, and W. Gibbons (1978), VLF electromagnetic waves observed onboard GEOS-1, *Space Sci. Rev.*, *22*, 371–382.
- Cornilleau-Wehrin, N., J. Solomon, A. Korth, and G. Kremser (1993), Generation mechanism of plasmaspheric ELF/VLF hiss: A statistical study from GEOS 1 data, *J. Geophys. Res.*, *98*, 21,471–21,479, doi:10.1029/93JA01919.
- Delport, B., A. B. Collier, J. Lichtenberger, C. J. Rodger, M. Parrot, M. A. Clilverd, and R. H. W. Friedel (2012), Simultaneous observation of chorus and hiss near the plasmopause, *J. Geophys. Res.*, *117*, A12218, doi:10.1029/2012JA017609.
- Dunckel, N., and R. A. Helliwell (1969), Whistler mode emissions on the OGO 1 satellite, *J. Geophys. Res.*, *74*, 6371–6385, doi:10.1029/JA074i026p06371.
- Gail, W. B., U. S. Inan, R. A. Helliwell, D. L. Carpenter, S. Krisnaswamy, T. J. Rosenberg, and L. J. Lanzerotti (1989), Characteristics of wave-particle interactions during sudden commencements, 1. Ground-based observations, *J. Geophys. Res.*, *95*, 119–137, doi:10.1029/JA095iA01p00119.
- Gail, W. B., and U. S. Inan (1990), Characteristics of wave-particle interactions during sudden commencements: 2. Spacecraft observations, *J. Geophys. Res.*, *95*, 139–147, doi:10.1029/JA095iA01p00139.
- Golden, D. I., M. Spasojevic, W. Li, and Y. Nishimura (2012), Statistical modeling of plasmaspheric hiss amplitude using solar wind measurements and geomagnetic indices, *Geophys. Res. Lett.*, *39*, L06103, doi:10.1029/2012GL051185.
- Gonzalez, W. D., J. A. Joselyn, Y. Kamide, H. W. Kroehl, G. Rostoker, B. T. Tsurutani, and V. M. Vasyliunas (1994), What is a geomagnetic storm?, *J. Geophys. Res.*, *99*, 5771–5792, doi:10.1029/93JA02867.
- Green, J. L., S. Boardsen, L. Garcia, W. W. L. Taylor, S. F. Fung, and B. W. Reinisch (2005), On the origin of whistler mode radiation in the plasmasphere, *J. Geophys. Res.*, *110*, A03201, doi:10.1029/2004JA010495.
- Gurnett, D. A., et al. (2004), The Polar plasma wave instrument, *Space Sci. Rev.*, *114*, 395–463.
- Hajra, R., E. Echer, B. T. Tsurutani, and W. D. Gonzalez (2013), Solar cycle dependence of High-Intensity Long-Duration Continuous AE Activity (HILDCAA) events, relativistic electron predictors?, *J. Geophys. Res. Space Physics*, *118*, 5626–5638, doi:10.1002/jgra.50530.
- Hajra, R., E. Echer, B. T. Tsurutani, and W. D. Gonzalez (2014), Superposed epoch analyses of HILDCAAs and their interplanetary drivers: Solar cycle and seasonal dependences, *J. Atmos. Sol. Terr. Phys.*, *121*, 24–31, doi:10.1016/j.jastp.2014.09.012.
- Hayakawa, M., and S. S. Sazhin (1992), Mid-latitude and plasmaspheric HISS-A review, *Planet. Space Sci.*, *40*, 1325–1338, doi:10.1016/0032-0633(92)90089-7.
- Kennel, C. F., and H. E. Petschek (1966), Limit on stably trapped particle fluxes, *J. Geophys. Res.*, *71*(1), 1–28, doi:10.1029/JZ071i001p00001.
- Kim, K.-C., D.-Y. Lee, and Y. Shprits (2015), Dependence of plasmaspheric hiss on solar wind parameters and geomagnetic activity and modeling of its global distribution, *J. Geophys. Res. Space Physics*, *120*, 1153–1167, doi:10.1002/2014JA020687.
- Kokubun, S. (1983), Characteristics of storm sudden commencements at geostationary orbit, *J. Geophys. Res.*, *88*, 10,025–10,0033, doi:10.1029/JA088iA12p10025.
- Korth, A., G. Kremser, N. Cornilleau-Wehrin, and J. Solomon (1986), Observations of energetic electrons and VLF waves at geostationary orbit during storm sudden commencements (SSC), in *Sol. Wind-Magn. Coupling*, edited by Y. Kamide and J. A. Slavin, pp. 391–399, Terra Sci., Tokyo.
- Lakhina, G. S., B. T. Tsurutani, O. P. Verkhoglyadova, and J. S. Pickett (2010), Pitch angle transport of electrons due to cyclotron interactions with coherent chorus subelements, *J. Geophys. Res.*, *117*, A00F15, doi:10.1029/2009JA014885.
- Li, W., et al. (2013), An unusual enhancement of low-frequency plasmaspheric hiss in the outer plasmasphere associated with substorm-injected electrons, *Geophys. Res. Lett.*, *40*, 3798–3803, doi:10.1002/grl.50787.

- Li, W., Q. Ma, R. M. Thorne, J. Bortnik, C. A. Kletzing, W. S. Kurth, G. B. Hospodarsky, and Y. Nishimura (2015), Statistical properties of plasmaspheric hiss derived from Van Allen Probes data and their effects on radiation belt electron dynamics, *J. Geophys. Res. Space Physics*, *120*, 3393–3405, doi:10.1002/2015JA021048.
- Lyons, L. R., R. M. Thorne, and C. F. Kennel (1972), Pitch angle diffusion of radiation belt electrons within the plasmasphere, *J. Geophys. Res.*, *77*, 3455–3474, doi:10.1029/JA077i019p03455.
- Lyons, L. R., and R. M. Thorne (1973), Equilibrium structure of radiation belt electrons, *J. Geophys. Res.*, *78*, 2142–2149, doi:10.1029/JA078i013p02142.
- Meredith, N. P., R. B. Horne, and R. R. Anderson (2001), Substorm dependence of chorus amplitudes: Implications for the acceleration of electrons to relativistic energies, *J. Geophys. Res.*, *106*, 13,165–13,13178, doi:10.1029/2000JA900156.
- Meredith, N. P., R. B. Horne, R. M. Thorne, D. Summers, and R. R. Anderson (2004), Substorm dependence of plasmaspheric hiss, *J. Geophys. Res.*, *109*, A06209, doi:10.1029/2004JA010387.
- Meredith, N. P., R. B. Horne, M. A. Clilverd, D. Horsfall, R. M. Thorne, and R. R. Anderson (2006), Origins of plasmaspheric hiss, *J. Geophys. Res.*, *111*, A09217, doi:10.1029/2006JA011707.
- Meredith, N. P., R. B. Horne, S. A. Glauert, and R. R. Anderson (2007), Slot region electron loss timescales due to plasmaspheric hiss and lightning-generated whistlers, *J. Geophys. Res.*, *112*, A08214, doi:10.1029/2007JA012413.
- Parrot, M., O. Santolik, N. Cornilleau-Wehrlin, M. Masimovic, and C. Harvey (2003), Magnetospherically reflected chorus waves revealed by ray tracing with CLUSTER data, *Ann. Geophys.*, *21*, 1111, doi:10.5194/angeo-21-1111-2003.
- Remya, B., B. T. Tsurutani, R. V. Reddy, G. S. Lakhina, and R. Hajra (2015), Electromagnetic cyclotron waves in the dayside subsolar outer magnetosphere generated by enhanced solar wind pressure: EMIC wave coherency (2015), *J. Geophys. Res. Space Physics*, *120*, 7536–7551, doi:10.1002/2015JA021327.
- Remya, B., K. H. Lee, L. C. Lee and B. T. Tsurutani (2016), Polarization of obliquely propagating whistler mode waves based on linear dispersion theory, *Phys. Plas.*, *23*, 122120, doi:10.1063/1.4972534.
- Roederer, J. G., and H. Zhang (2014), *Dynamics of Magnetically Trapped Particles-Foundations of the Physics of Radiation Belts and Space Plasmas*, Springer Verlag, New York.
- Russell, C. T., R. E. Holzer, and E. J. Smith (1969), Observations of ELF noise in the magnetosphere, 1. Spatial extent and frequency of occurrence, *J. Geophys. Res.*, *74*, 755–777, doi:10.1029/JA074i003p00755.
- Santolik, O., M. Parrot, L. R. O. Storey, J. S. Pickett, and D. A. Gurnett (2001), Propagation analysis of plasmaspheric hiss using Polar PWI measurements, *Geophys. Res. Lett.*, *28*, 1127–1130, doi:10.1029/2000GL012239.
- Santolik, O., J. Chum, M. Parrot, D. A. Gurnett, J. S. Pickett, and N. Cornilleau-Wehrlin (2006), Propagation of whistler mode chorus to low altitudes: Spacecraft observations of structured ELF hiss, *J. Geophys. Res.*, *111*, A10208, doi:10.1029/2005JA011462.
- Santolik, O. (2008), New results of investigations of whistler-mode chorus emissions, *Nonl. Proc. Geophys.*, *15*, 621, doi:10.5194/npg-15-621-2008.
- Santolik, O., and J. Chum (2009), The origin of plasmaspheric hiss, *Science*, *324*(5928), 729, doi:10.1126/science.1172878.
- Shinbori, A., T. Ono, M. Iizima, and A. Kumamoto (2003), Sudden commencements related plasma waves observed by the Akebono satellite in the polar region and inside the plasmasphere region, *J. Geophys. Res.*, *108*(A12), 1457, doi:10.1029/2003JA009964.
- Smith, E. J., and B. T. Tsurutani (1976), Magnetosheath lion roars, *J. Geophys. Res.*, *81*, 2261–2266, doi:10.1029/JA081i013p02261.
- Smith, E. J., and J. H. Wolfe (1976), Observations of interaction regions and corotating shocks between one and five AU: Pioneers 10 and 11, *Geophys. Res. Lett.*, *3*, 137–140, doi:10.1029/GL003i003p00137.
- Smith, E. J., A. M. A. Frandsen, B. T. Tsurutani, R. M. Thorne, and K. W. Chan (1974), Plasmaspheric hiss intensity variations during magnetic storms, *J. Geophys. Res.*, *79*, 2507–2510, doi:10.1029/JA079i016p02507.
- Solomon, J., N. Cornilleau-Wehrlin, A. Korth, and G. Kremser (1988), An experimental study of ELF/VLF hiss generation in the Earth's magnetosphere, *J. Geophys. Res.*, *93*, 1839–1847, doi:10.1029/JA093iA03p01839.
- Spasojevic, M., Y. Y. Shprits, and K. Orlova (2015), Global empirical models of plasmaspheric hiss using Van Allen probes, *J. Geophys. Res. Space Physics*, *120*, 10,370–10,383, doi:10.1002/2015JA021803.
- Storey, L. R. O., F. Lefeuvre, M. Parrot, L. Cairo, and R. R. Anderson (1991), Initial survey of the wave distribution functions for plasmaspheric hiss observed by ISEE-1, *J. Geophys. Res.*, *96*, 19,469–19,19489, doi:10.1029/91JA01828.
- Summers, D., Y. Omura, S. Nakamura, and C. A. Kletzing (2014), Fine structure of plasmaspheric hiss, *J. Geophys. Res. Space Physics*, *119*, 9134–9149, doi:10.1002/2014JA020437.
- Thorne, R. M., E. J. Smith, R. K. Burton, and R. E. Holzer (1973), Plasmaspheric hiss, *J. Geophys. Res.*, *78*, 1581–1596, doi:10.1029/JA078i010p01581.
- Thorne, R. M., E. J. Smith, K. J. Fiske, and S. R. Church (1974), Intensity variation of ELF hiss and chorus during isolated substorms, *Geophys. Res. Lett.*, *1*, 193–196, doi:10.1029/GL001i005p00193.
- Thorne, R. M., S. R. Church, W. J. Malloy, and B. T. Tsurutani (1977), The local time variation of ELF emissions during periods of substorm activity, *J. Geophys. Res.*, *82*, 1585–1590, doi:10.1029/JA082i010p01585.
- Thorne, R. M., S. R. Church, and D. J. Gorney (1979), On the origin of plasmaspheric hiss: The importance of wave propagation during periods of substorm activity, *J. Geophys. Res.*, *84*, 5241–5247, doi:10.1029/JA084iA09p05241.
- Tsurutani, B. T., and W. D. Gonzalez (1987), The cause of high-intensity long-duration continuous AE activity (HILDCAAS): Interplanetary Alfvén wave trains, *Planet. Space Sci.*, *35*(4), 405, doi:10.1016/0032-0633(87)90097-3.
- Tsurutani, B. T., and W. D. Gonzalez (1997), The interplanetary causes of magnetic storms: A review, in *Magnetic Storms*, vol. 98, edited by B. T. Tsurutani et al., pp. 77, AGU Press, Washington, D. C.
- Tsurutani, B. T., and G. S. Lakhina (1997), Some basic concepts of wave-particle interactions in collisionless plasmas, *Rev. Geophys.*, *35*(4), 491–502.
- Tsurutani, B. T., and E. J. Smith (1974), Postmidnight chorus: A substorm phenomenon, *J. Geophys. Res.*, *79*, 118–127, doi:10.1029/JA079i001p00118.
- Tsurutani, B. T., and E. J. Smith (1977), Two types of magnetospheric ELF chorus and their substorm dependences, *J. Geophys. Res.*, *82*, 5112–5128, doi:10.1029/JA082i032p05112.
- Tsurutani, B. T., E. J. Smith, and R. M. Thorne (1975), Electromagnetic hiss and relativistic electron losses in the inner zone, *J. Geophys. Res.*, *80*, 600–607, doi:10.1029/JA080i004p00600.
- Tsurutani, B. T., W. D. Gonzalez, A. L. C. Gonzalez, F. Tang, J. K. Arballo, and M. Okada (1995), Interplanetary origin of geomagnetic activity in the declining phase of the solar cycle, *J. Geophys. Res.*, *100*, 21,717–21,733, doi:10.1029/95JA01476.
- Tsurutani, B. T., W. D. Gonzalez, F. Guarnieri, Y. Kamide, X.-Y. Zhou, and J. K. Arballo (2004), Are high-intensity, long-duration continuous AE activity (HILDCAA) events substorm expansion events?, *J. Atmos. Sol. Terr. Phys.*, *66*, 167, doi:10.1016/j.jastp.2003.08.015.

- Tsurutani, B. T., et al. (2006), Corotating solar wind streams and recurrent geomagnetic activity: A review, *J. Geophys. Res.*, *111*, A07S01, doi:10.1029/2005JA011273.
- Tsurutani, B. T., E. Echer, F. L. Guarnieri, and J. U. Kozyra (2008), CAWSES November 7–8, superstorm: Complex solar and interplanetary features in the post-solar maximum phase, *Geophys. Res. Lett.*, *35*, L06S05, doi:10.1029/2007GL031473.
- Tsurutani, B. T., O. P. Verkhoglyadova, G. S. Lakhina, and S. Yagitani (2009), Properties of dayside outer zone chorus during HILDCAA events (2009): Loss of energetic electrons, *J. Geophys. Res.*, *114*, A03207, doi:10.1029/2008JA013353.
- Tsurutani, B. T., B. J. Falkowski, O. P. Verkhoglyadova, J. S. Pickett, O. Santolik, and G. S. Lakhina (2011a), Quasi-coherent chorus properties: 1. Implications for wave-particle interactions, *J. Geophys. Res.*, *116*, A09210, doi:10.1029/2010JA016237.
- Tsurutani, B. T., E. Echer, and W. D. Gonzalez (2011b), The solar and interplanetary causes of the recent minimum in geomagnetic activity (MGA23): A combination of midlatitude small coronal holes, low IMF Bz variances, low solar wind speeds and low solar magnetic fields, *Ann. Geophys.*, *29*, 839–849, doi:10.5194/angeo-29-1-2011.
- Tsurutani, B. T., B. J. Falkowski, O. P. Verkhoglyadova, J. S. Pickett, O. Santolik, and G. S. Lakhina (2012), Dayside ELF electromagnetic wave survey: A Polar statistical study of chorus and hiss, *J. Geophys. Res.*, *117*, A00L12, doi:10.1029/2011JA017180.
- Tsurutani, B. T., G. S. Lakhina, and O. P. Verkhoglyadova (2013), Energetic electron (>10 keV) microburst precipitation, ~5–15 s X-ray pulsations, chorus and wave-particle interactions: A review, *J. Geophys. Res. Space Physics*, *118*, 2296–2312, doi:10.1002/jgra.50264.
- Tsurutani, B. T., B. J. Falkowski, J. S. Pickett, O. P. Verkhoglyadova, O. Santolik, and G. S. Lakhina (2014a), Extremely intense ELF magnetosonic waves: A survey of Polar observations, *J. Geophys. Res. Space Physics*, *119*, 964–977, doi:10.1002/2013JA019284.
- Tsurutani, B. T., E. Echer, K. Shibata, O. P. Verkhoglyadova, A. J. Mannucci, W. D. Gonzalez, J. U. Kozyra, and M. Pätzold (2014b), The interplanetary causes of geomagnetic activity during the 7–17 March 2012 interval: A CAWSES II overview, *J. Spa. Weath. Spa. Clim.*, *4*, A02-p1 to A02-p8, doi:10.1051/swsc/2013056.
- Tsurutani, B. T., B. J. Falkowski, J. S. Pickett, O. Santolik, and G. S. Lakhina (2015), Plasmaspheric hiss properties: Observations from Polar, *J. Geophys. Res. Space Physics*, *120*, 414–431, doi:10.1002/2014JA020518.
- Tsurutani, B. T., et al. (2016), Heliospheric plasmashet (HPS) impingement onto the magnetosphere as a cause of relativistic electron dropouts (REDs) via coherent EMIC wave scattering with possible consequences for climate change, *J. Geophys. Res. Space Physics*, *121*, 10,130–10,156, doi:10.1002/2016JA022499.
- Verkhoglyadova, O. P., B. T. Tsurutani, and G. S. Lakhina (2010), Properties of obliquely propagating chorus, *J. Geophys. Res.*, *115*, A00F19, doi:10.1029/2009JA014809.
- Verkhoglyadova, O. P., A. J. Mannucci, B. T. Tsurutani, M. G. Mlynarczyk, L. A. Hunt, R. J. Redmon, and J. C. Green (2016), Localized thermosphere ionization events during the high-speed stream interval of 29 April to 5 May 2011, *J. Geophys. Res. Space Physics*, *120*, 675–696, doi:10.1002/2014JA020535.
- Wang, C., Q. Zong, F. Xiao, Z. Su, Y. Wang, and C. Yue (2011), The relations between magnetospheric chorus and hiss inside and outside the plasmasphere boundary layer: Cluster observation, *J. Geophys. Res.*, *116*, A07221, doi:10.1029/2010JA016240.